ELSEVIER

Polymer 41 (2000) 2639–2646

polymer

Study of the crystallization behaviors of polypropylene and maleic anhydride grafted polypropylene

Yongsok Seo[a,*], Jinho Kim[a], Kwang Ung Kim[a], Young Chul Kim[b]

[a]*Polymer Processing Laboratory, Korea Institute of Science and Technology (KIST), P.O. Box 131, Cheongryang, Seoul, South Korea*
[b]*Polymer Materials Laboratory, Korea Institute of Science and Technology (KIST), P.O. Box 131, Cheongryang, Seoul, South Korea*

Received 2 September 1998; received in revised form 16 November 1998; accepted 20 May 1999

Abstract

The crystallization kinetics of isotactic polypropylene (iPP) and maleic anhydride grafted polypropylene (MA–PP) and their blends, crystallized both nonisothermally and isothermally, were investigated by differential scanning calorimetry. During isothermal crystallization, relative crystallinity developed with the time dependence described by the Avrami equation with exponents $n \approx 2.7$ for neat iPP and $n \approx 3.8$ for MA–PP. The half crystallization time for MA–PP was much smaller than that for iPP. The half crystallization time of iPP depended more strongly on the crystallization temperature than that of MA–PP did. A kinetic equation for nonisothermal crystallization was employed to analyze the crystallization characteristics of iPP and MA–PP. The nonisothermal crystallization kinetic analysis for MA–PP at different cooling rates was possible, assuming that the spherulitic growth was initiated by heterogeneous nucleation alone while that for iPP at high cooling rates was successfully done by assuming both homogeneous and heterogeneous nucleations. The diffusional activation energy was smaller for MA–PP than for iPP. The number of heterogeneous nuclei for MA–PP was larger than that for iPP. The presence of MA–PP in iPP affects the crystallization of iPP by acting as a nucleating agent.

Keywords: Polypropylene; Crystallization kinetics; Avrami equation

1. Introduction

The physical properties of semi-crystalline polymeric materials strongly depend on their microstructure and crystallinity, because failure of the materials takes place at the microscopic level. The crystalline form can be obtained by slowly cooling the melt or by isothermal crystallization at a temperature between the crystalline melting point and the glass transition temperature. From this point of view, the crystallization kinetics of isotactic polypropylene (iPP) has been widely studied by different methods. Isothermal crystallization kinetics, in general, has been well described by the Avrami equation [1–12] though it is limited when used to describe the crystallization of a nucleated iPP whose crystallinity increases rapidly due to numerous crystallization sites. Maleic anhydride grafted polypropylene (MA–PP), which has been widely used for in situ or reactive compatibilization, has the same molecular structure as polypropylene except for the maleic anhydride group being attached to the backbone [13]. Recently, we used it in a blend of poly(amide) (nylon6) and a thermotropic liquid crystalline polymer (poly(ester amide)) to make a kind of in situ compatibilizer which was produced by using extrusion process and which acted at the interface to reduce the interfacial tension between the matrix (nylon6) and the dispersed thermotropic liquid crystalline phase [14–16]. It was observed that MA–PP partly acts as a nucleating agent for the matrix [16]. This was intriguing because the maleated polypropylene was interacting with both phases and acted as a nucleating agent, which definitely affected the final properties of the blends. Though the main structure of MA–PP is similar to that of iPP, its crystallization behavior has yet to be studied in detail. This subject is of great importance, since the use of MA–PP in conjunction with iPP is becoming more and more frequent.

This study investigates the crystallization behavior of MA–PP and iPP. Both isothermal and non-isothermal crystallization processes were employed. The Avrami equation and a non-isothermal crystallization kinetic equation were used for the analysis. Dynamic differential scanning calorimetry (DSC) thermograms provided the necessary data. Polarized optical microscope observations were also made

* Corresponding author.

0032-3861/00/$ - see front matter
PII: S0032-3861(99)00425-5

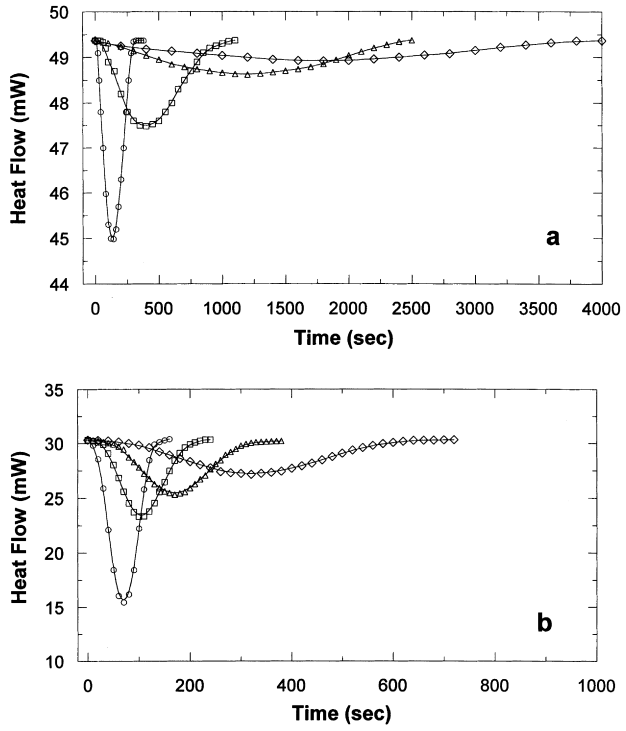

Fig. 1. Heat flow versus time during isothermal crystallization. (a) iPP at 120°C (○), 125°C (□), 130°C (△), and 132°C (◇), and (b) MA–PP at 125°C (○), 130°C (□), 132°C (△), and 135°C (◇).

to see the effect of different structures on the crystallization behavior.

2. Experimental

2.1. Materials and instrumentation

Both commercial grade iPP powder and MA–PP powder without any additives were supplied by Honam Petrochemical Co. (Korea). Their number-average and weight-average molecular weights were known to be 4.18×10^4 and 2.3×10^5 g/mol, respectively. The maleic anhydride content was known to be 1 wt%. First, coarse particles in the as-received powders were removed by sieving them with a No.100 standard sieve (mesh size = 150 μm). The MA–PP powder was reprecipitated in methanol and washed with ethanol and acetone twice. The powders were dried in a vacuum oven at 60°C for 72 h.

Dynamic crystallization was carried out in the sample pan of a Perkin–Elmer DSC-7 calorimeter. The standard procedure for the DSC is as follows: the samples (about 7 mg) were melted at 200°C for 10 min in order to eliminate any previous thermal history; then they were rapidly cooled to the crystallization temperature, T_c, and maintained at that temperature during the time necessary for isothermal crystallization. The crystallization temperatures were selected so as to compare our data with those of other experiments [5,10]. For dynamic non-isothermal crystallization, the samples were melted at 200°C for 10 min and then cooled at a constant cooling rate.

The morphologies of the resins on thin films were studied by using an optical polarizing microscope (Samsung MW, Korea) with a Mettler FP-90 automatic hot-stage thermal controller. The samples were sandwiched between microscope cover slips, melted at 200°C for 10 min in a separate hot stage, and then rapidly moved to another hot stage which was equipped with the microscope and which was set to the crystallization temperature.

Melt blending of iPP and MA–PP was done in an Axon single screw extruder (Plastmaskiner BX-10). The extrusion temperatures were 140, 200 and 200°C for the hopper, the melting zone and the die, respectively.

2.2. The crystallization kinetic equation

The isothermal crystallization kinetics of a material can be analyzed by evaluating its degree of crystalline conversion as a function of time at a constant temperature. The variation of the crystallinity is related to the ratio of the heat generated at time t to the heat generated at infinite time according to the equation [5,6]

$$X(t) = Q_t/Q_\infty = \int_0^t (\mathrm{d}H/\mathrm{d}t)\,\mathrm{d}t \Big/ \int_0^\infty (\mathrm{d}H/\mathrm{d}t)\,\mathrm{d}t \tag{1}$$

where $\mathrm{d}H/\mathrm{d}t$ is the rate of heat evolution. Development of relative crystallinity can be analyzed using the Avrami equation [7–9]

$$X(t)/X(\infty) = 1 - \exp(-k_n t^n) \tag{2}$$

This equation can be changed to

$$\ln(1 - X(t)/X(\infty)) = -k_n t^n \tag{3a}$$

$$\log[-\ln(1 - X(t)/X(\infty))] = n \log t + \log k_n/2.303 \tag{3b}$$

where n is a constant whose value depends on the mechanism of nucleation and on the form of crystal growth, k_n is a constant containing the nucleation and the growth parameters. From a graphic representation of $\log[-\ln(1 - X(t))]$ versus $\log t$, the Avrami coefficient n (slope of the straight line) and the crystallization kinetic constant k_n (intersection with the y-axis) can be calculated. However, the value of k_n is very often obtained from the equation [17]

$$k_n = \ln 2/t_{1/2}^n \tag{4}$$

where $t_{1/2}$ is the half-time of crystallization.

The nonisothermal crystallization kinetic equation used was the one based upon the theory of phase-transition kinetics with growth-site impingement. The equation is a linear combination of two terms involving the growth process initiated by heterogeneous and homogeneous

Table 1
Kinetic parameters from the analysis of isothermal crystallization

	T (°C)	n	log k	$t_{1/2}$ (s)
iPP	120	2.68	−6.2	176
	125	2.73	−7.5	488
	130	2.69	−8.4	1201
	132	2.66	−8.9	1876
MA–PP	125	3.74	−7.2	77
	130	3.77	−8.3	147
	132	3.93	−9.2	204
	135	3.83	−10.1	378

nucleation [19,20],

$$\alpha(t) = \alpha_1(t) + \alpha_2(t)$$

$$= k_1 \exp\left(-\frac{3E_d}{RT}\right)\exp\left(-\frac{3\Psi_1 T_m^0}{fT(T_m^0 - T)}\right)t^2(1-\alpha(t))^2$$

$$+k_2 \exp\left(-\frac{4E_d}{RT}\right)\exp\left(-\frac{\Psi_2 (T_m^0)^2}{f^2 T(T_m^0 - T)^2} - \frac{3\Psi_1 T_m^0}{fT(T_m^0 - T)}\right)$$

$$\times t^2(1-\alpha(t))^2 \int_0^t (t-\omega)^2[1-\alpha(\omega)]\,d\omega \quad (5)$$

where $\alpha(t)$ is the overall crystallization rate at time t, $\alpha_1(t)$ is the contribution to the crystallization rate due to the growth process initiated by heterogeneous nucleation, $\alpha_2(t)$ is the contribution to the crystallization rate due to the growth process initiated by homogeneous nucleation, T_m^0 is the equilibrium melting temperature, and $f = 2T/T_m^0 + T$). There are five independent parameters; k_1 is the rate constant for $\alpha_1(t)$, which is proportional to the effective number of nuclei; E_d is the diffusional activation energy of the crystallizing segments across the phase boundary; ψ_1 is a constant related to the free energy of formation of a critical nucleus on the growing crystal surface; k_2 is the rate constant for the $\alpha_2(t)$ term; and ψ_2 is a constant related to the free energy of formation of a growth embryo in the homogeneous nucleation process.

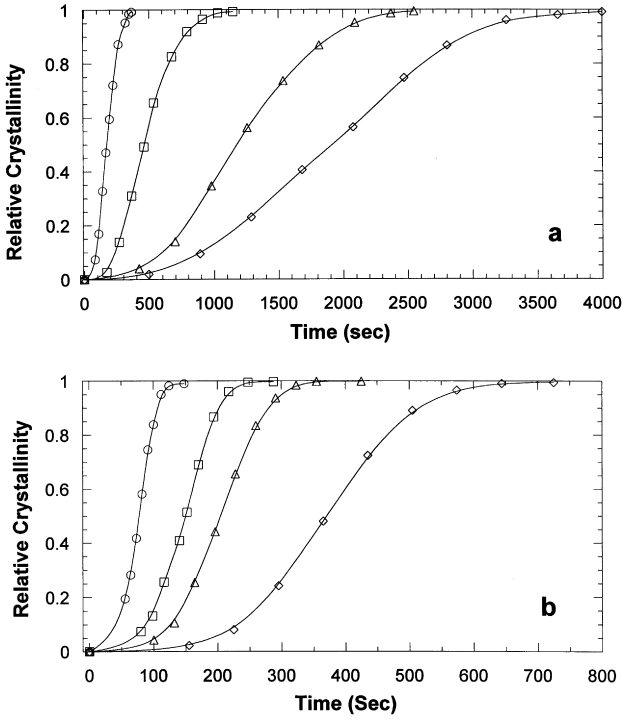

Fig. 2. Development of relative crystallinity with time for isothermal crystallization (a) iPP at 120°C (○), 125°C (□), 130°C (△), and 132°C (◇), and (b) MA–PP at 125°C (○), 130°C (□), 132°C (△), and 135°C (◇).

3. Results and discussion

In order to analyze the effect of temperature on the crystallization, the crystallization isotherms of iPP and MA–PP at different crystallization temperatures are graphically presented in Fig. 1. As can be seen, the time to reach the maximum degree of crystalline order in iPP and MA–PP increases as the crystallization temperature increases. MA–PP reaches the maximum degree of crystalline order earlier than iPP. This is manifested more at high crystallization temperatures. As explained later, this is ascribed to the differences in the crystallization processes for iPP and MA–PP. The number of nuclei in MA–PP is much larger than that in iPP; thus, crystallization of MA–PP proceeds mainly via heterogeneous nucleation while that of iPP proceeds both by heterogeneous and homogeneous nucleation mechanisms. Since homogeneous nucleation starts spontaneously by chain aggregation below the melting point [4,5] it requires a longer time, whereas heterogeneous nuclei form simultaneously as soon as the sample reaches the crystallization temperature. Homogeneous nucleation, therefore, requires more time at higher crystallization temperatures. Thus, the time to reach the maximum degree of crystalline order in iPP is longer than that in MA–PP.

Table 1 presents a summary of the crystallinity and the time data for isothermal crystallization from the melt-state. The time $t_{1/2}$ represents the time to reach the maximum rate of heat flow and corresponds to the change over to a slower kinetic process due to impingement of adjacent spherulites [17]. Crystallization continues until the time after which no further heat flow is observed. The relative amount of crystallinity for iPP and MA–PP has been plotted in Fig. 2 for four crystallization temperatures. Fig. 2 also shows that MA–PP crystallizes faster than iPP. Plots of $\log[-\ln(1 - X(t)/X(\infty))]$ versus $\log t$ are shown in Fig. 3. Each curve shows only the linear portion, which is followed by a gentle roll-off at longer times. Small deviations from linearity in the short-time region where logarithmic plotting tends to exaggerate small errors in the assignment of the start of crystallization were removed in order to show the proportional region more clearly. The relative crystallinity range over which the data are presented was limited to 40%. This region was arbitrarily chosen assuming that at low degrees

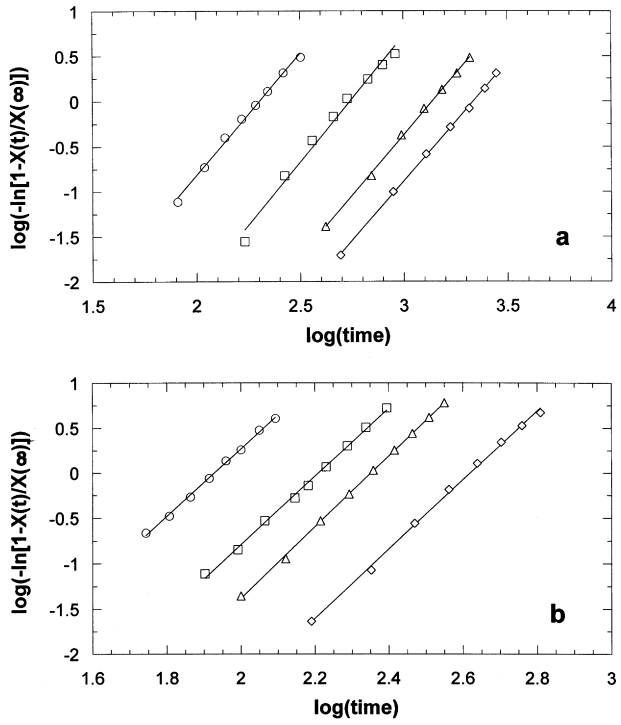

Fig. 3. Plot of $\log[-\ln(1 - X(t)/x(\infty))]$ versus $\log t$ for isothermal crystallization. (a) iPP at 120°C (○), 125°C (□), 130°C (△), and 132°C (◇), and (b) MA–PP at 125°C (○), 130°C (□), 132°C (△), and 135°C (◇).

of relative crystallinity growth-site impingement, which also makes the Avrami equation deviate from linearity [7,8], does not have a significant effect on the spherulite growth.

The Avrami equation with the kinetic parameters so determined as to fit the early-stage data predicts a higher conversion into crystals at longer times [18]. The Avrami exponents for iPP are about 2.69 ± 0.03 over the crystallization temperature range studied. From these values of the Avrami exponents, it can be established that spherulitic development arises from an athermal and instantaneous nucleation, even though the growth rate is not constant as deduced from the non-integer value of n [9,18]. The intercept

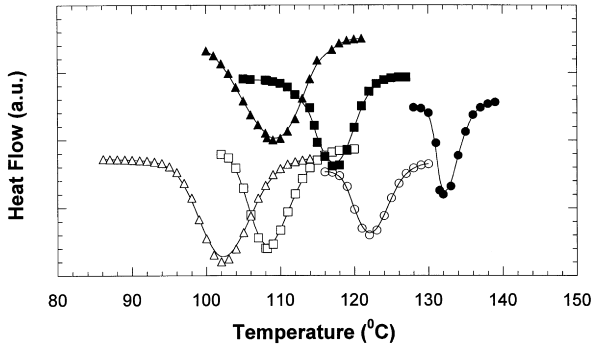

Fig. 4. Effect of the cooling rate on crystallization exotherm. Samples were heated to 200°C and held for 10 min, then cooled at the indicated cooling rates. iPP at −1°C/min (○), −10°C/min (□), and −20°C/min (△), and MA–PP at −1°C/min (●), −10°C/min (■), and −20°C/min (▲).

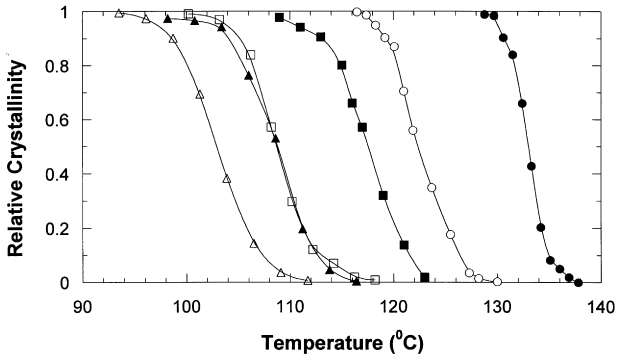

Fig. 5. Development of the relative crystallinity versus temperature during nonisothermal crystallization at the indicated cooling rates. iPP at −1°C/min (○), −10°C/min (□), and −20°C/min (△), and MA–PP at −1°C/min (●), −10°C/min (■), and −20°C/min (▲). The lines are guides for the eye.

value ($\log k_n$) decreases with increasing crystallization temperature, which means a decrease in the nucleation rate constant and in the growth constant. The half time of iPP crystallization ($t_{1/2}$) increases with the crystallization temperature (hence a smaller supercooling temperature) in agreement with earlier observations [3,5]. The Avrami exponents for MA–PP are about 3.82 ± 0.08 over the crystallization temperature range studied. These values are noticeably different from those of iPP [2,5,9]. From these values, it can be speculated that spherulitic development of the MA–PP crystalline phase arises from an athermal and random nucleation [17,18], even though the growth rate is not constant. An increase in the Avrami exponent is usually attributed in the literature to a change from instantaneous to sporadic nucleation [2,6,17,18]. The intercept value ($\log k_n$) decreases with increasing crystallization temperature, which also means a decrease in the nucleation rate constant and in the growth constant. The half time of MA–PP crystallization ($t_{1/2}$) increases with the crystallization temperature, but at a much slow rate compared to iPP, which means the dependence of the crystallization kinetics on the crystallization temperature is much weaker for MA–PP than for iPP. This can be ascribed to the heterogeneous nucleation of MA–PP, which is less temperature dependent [17]. This is addressed later in connection with the nonisothermal crystallization behaviors of iPP and MA–PP.

The crystallization of iPP and MA–PP was also investigated under nonisothermal conditions of heating and cooling. They were crystallized from the melt by cooling from 200°C at rates of 1, 10 and 20°C/min. The results are shown in Fig. 4. The exothermic peak on cooling shifts to lower temperatures as the heating rate decreases. The maximum rate of heat flow for iPP occurs at temperatures of 122, 108 and 102°C for a cooling rate of −1, −10 and −20°C/min, respectively, while that for MA–PP occurs at temperatures of 132, 117 and 109°C for a cooling rate of −1, −10 and −20°C/min, respectively. At a constant cooling rate, relative crystallinity develops with temperature as shown in Fig. 5. Integration of the exothermic peaks during the

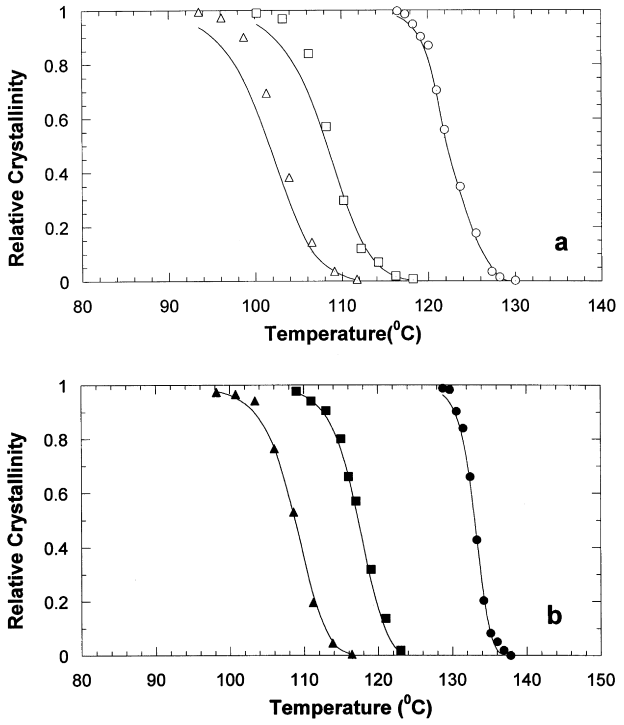

Fig. 6. Comparison of the relative crystallinity changes. (a) iPP at −1°C/min (○), −10°C/min (□), and −20°C/min (△), and MA–PP at −1°C/min (●), −10°C/min (■), and −20°C/min (▲).The lines are theoretical calculation from Eq. (5) using only the heterogeneous nucleation term.

nonisothermal scan gives sigmoidal curves characterized by a fast 'primary' process during the initial stages and by slower 'secondary' processes during the later stages [10,11]. During the nonisothermal scans, the crystallization is enhanced as temperature decreases. This is because of the strong temperature dependence of the nucleation and the growth parameters. Thus, after the maximum in the heat flow curve has been passed, a large fraction of crystallinity develops by slower, secondary kinetic processes. A slow cooling rate provides more fluidity and diffusivity for the molecules due to low viscosity and more time for the secondary crystallization, thus inducing more crystallinity at higher temperatures than for the samples cooled with fast cooling rates, as shown in Fig. 5. The inflection point in each curve represents the temperature corresponding to the maximum rate of heat flow (the peak temperature in Fig. 4). The inflection point occurs at a decreasing degree of conversion as the cooling rate increases. The relative crystallinity that develops at the peak temperature is slightly decreased with cooling rates. This is more noticeable for MA–PP, which means MA–PP crystallizes more when the cooling proceeds more slowly. The effects of the hydrogen bonding and the ordering of conformation appear more clearly when enough time is provided for reaction.

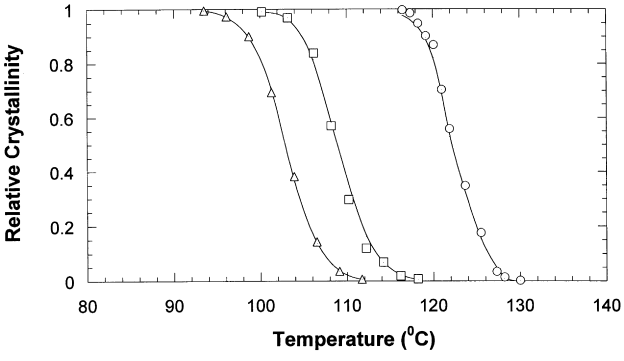

Fig. 7. Comparison of the relative crystallinity changes for iPP using both the heterogeneous nucleation term and the homogeneous nucleation term. Cooling rates are −1°C/min (○), −10°C/min (□), and −20°C/min (△), respectively.

In studying the crystallization kinetics of semicrystalline polymers, the equilibrium melting temperature (T_m^0) of iPP needs to be known in order to compute the degree of supercooling [5,18–20]. To estimate T_m^0, 0.3 mm-thick iPP and MA–PP films were isothermally crystallized at various temperatures between 110 and 140°C in the DSC sample pan after premelting at 200°C for 10 min. After crystallization at a predetermined temperature, the melting temperature was obtained by reheating the samples at a rate of 10°C/min. It was possible to calculate the equilibrium melt temperature (T_m^0) for iPP by plotting T_c versus T_m and observing the intersection of this line with a line having a slope equal to one ($T_m = T_c$) (Hoffman–Weeks plot). The corresponding values of T_m^0 for iPP and MA–PP were determined as 209 and 218°C, respectively. Different T_m^0 values have been reported in the literature [4,5]. A complex behavior was observed when iPP was crystallized below 125°C, and a deflection point appeared depending on the crystallization temperature [4,17–19]. A deflection was also observed by Kim et al. [19] and Cheng et al. [4] and besides the molecular factors such as molecular weight and the degree of stereo-regularity, it is considered as one of the reasons for the large scattering in the experimental T_m^0 data [4,5,17,18].

The nonisothermal crystallization kinetic equation is a linear combination of two terms involving the growth processes initiated by heterogeneous nucleation ($\alpha_1(t)$) and by homogeneous nucleation ($\alpha_2(t)$). The overall crystallization rate is affected by both the processes. Since their effects are mutually compensating, separate investigations of these effects are done. In the region near the melting point, the homogeneous nucleation and growth process is considerably delayed because the free energy of formation of a growth embryo is very high [18,21]. In this case, the heterogeneous nucleation and growth process controls the rate of crystallization. At high crystallization temperatures or at low cooling rates (1°C/min), it is reasonable to assume that $\alpha_1(t)$ is much greater than $\alpha_2(t)$. First, the relative crystallinity changes measured from DSC thermograms were fitted using only the heterogeneous crystallization term ($\alpha_1(t)$). Fig. 6 shows the result of regression fits for iPP and MA–PP at cooling rates of 1, 10, and 20°C/min, respectively. When the cooling rate is low (1°C/min), the regression

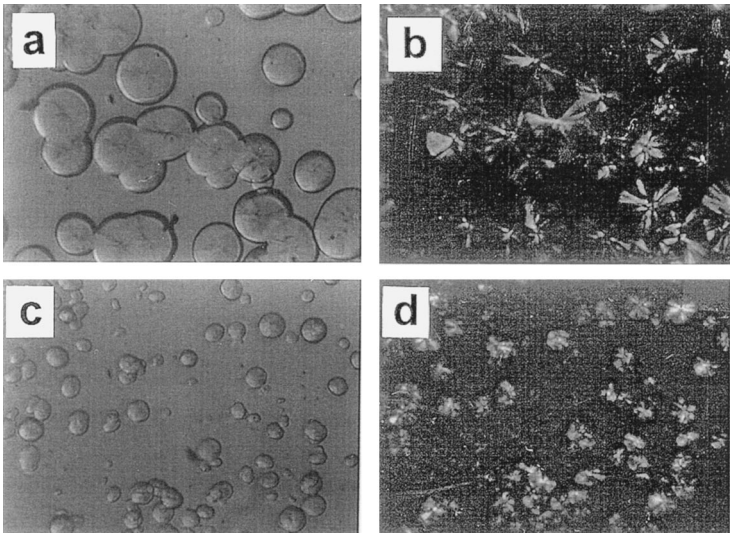

Fig. 8. Morphology of crystallized iPP ((a) semi-polarized and (b) polarized pictures), and 0.2%MA–PP added iPP ((c) semi-polarized and (d) polarized pictures). These pictures were taken at the same time (50 s after the crystallization was started) and temperature (125°C).

fitting of Eq. (5) to the experimental data provides a good correlation for both iPP and MA–PP. When the samples are crystallized at high cooling rates of 10 and 20°C/min, some discrepancy occurs between the experimental data and the calculated values for iPP while good agreement is still observed for MA–PP. This is thought to be due to different nucleation processes occurring in iPP and MA–PP. At higher cooling rates, nucleation in MA–PP proceeds mostly by a heterogeneous process while in iPP it occurs via two competing nucleation processes, i.e. homogeneous and heterogeneous processes. Fig. 7 shows the finer fit of the iPP data when the contribution of the $\alpha_2(t)$ term in Eq. (5) is included in the regression at various cooling rates. The experimental and the calculated results show good agreement, which supports our speculation and indicates that the model equation is appropriate for describing the nonisothermal crystallization kinetics of iPP.

Because of the complex temperature dependence of the rate constant and the peculiar features of crystallization, a determination of the kinetic characteristics from nonisothermal studies is useful only in a qualitative analysis [19,22]. Also, there are some risks involved in using a nonlinear regression technique to fit theoretically derived models to experimental data [20,23]. By evaluating the parameters in the model, however, we may get a glimpse of the different crystallization behaviors of iPP and MA–PP. The kinetic parameters, k_1, E_d, and ψ_1 in the $\alpha_1(t)$ term of Eq. (5) were 2.09×10^{24} s^{-3}, 3200 cal/mol and 1.09×10^3 K, respectively, for iPP and 1.89×10^{25} s^{-3}, 2730 cal/mol, and 1.09×10^3 K, respectively, for MA–PP. Since the rate constant k_1 for $\alpha_1(t)$ is proportional to the number of effective nuclei, it is reasonable to say that the number of nuclei for MA–PP is almost ten times higher than for iPP. This might be due to the associated chains through some interactions such as hydrogen bonding between hydrolyzed maleic anhydride groups in different chains and/or some additives used for grafting the maleic anhydride to the iPP backbone. The former is considered a more plausible reason, because it was recently reported by Kim et al. [22] that fitting of isothermally nucleated iPP (the same iPP as used in this study) yielded Avrami exponent values of about 3.2 at a temperature of 136°C. The diffusional activation energy of MA–PP is also much lower than that of iPP, which means diffusion of the crystallizing elements across the phase boundary is easier for MA–PP. On the contrary, the ψ_1 value of MA–PP is similar than that of iPP, which means the free energy of formation of a critical nucleus on the growing crystal surface is almost the same for the two materials. The good agreement between the experimental data and the calculated values for MA–PP, which was obtained by using only the heterogeneous nucleation term, can be ascribed to this large number of existing nuclei and low diffusional activation energy. When the contribution of the homogeneous nucleation term, $\alpha_2(t)$, was included in the regressional fitting of the iPP data, the kinetic parameters, k_2 and ψ_2, in the $\alpha_2(t)$ term of Eq. (5) were 2.18×10^{46} s^{-3} and 0.91×10^3 K, respectively. The value of k_2 is much larger than the value of k_1, thus, the contribution of the $\alpha_2(t)$ term to the overall crystallization rate will be important when the cooling rate is high. The value of ψ_2 is close to ψ_1, which is different from Kim et al.'s result [19], but is in good agreement with Hammami and Mehrotra's evaluation [20]. As explained in Hammami and Mehrotra's paper, this is ascribed to a difference in the theoretical expression for the homogeneous nucleation rate. Also, this may imply that the rate of homogeneous nucleation is not that much slower than the rate of secondary nucleation on the growing crystal surface [20,21].

Since the crystallization behavior of MA–PP is different from that of iPP, it is intriguing to see the effect of MA–PP

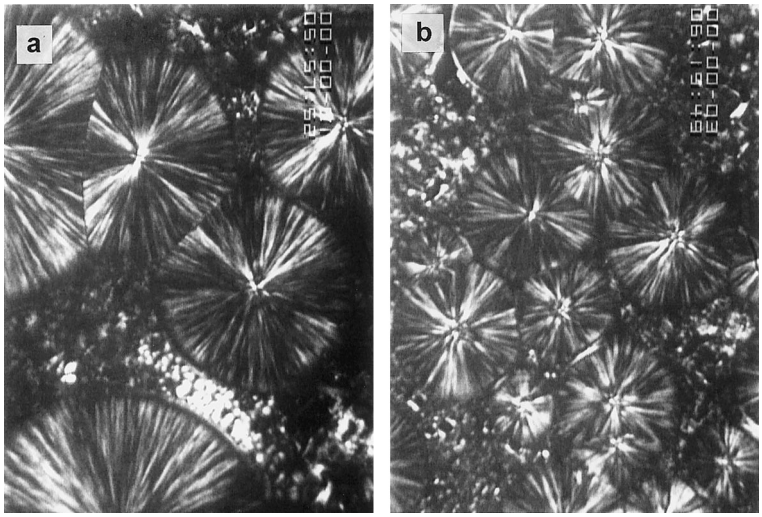

Fig. 9. Morphology of crystallized iPP (a) and 0.2% MA–PP added iPP (b) after the completion of the crystallization at 125°C.

addition to iPP. Fig. 8 shows the micrographs and the polarized micrographs of iPP and iPP with 0.2% MA–PP added. The iPP with MA–PP added shows more spherulitic sites and a finer morphology, indicating that MA–PP acts as a nucleating agent. MA–PP addition accelerates the nucleation, but the radial growth rate of the spherulites decreases slightly down with the addition of MA–PP. Fig. 9 shows the enlarged polarized micrographs taken when the crystallization was complete. Addition of MA–PP rapidly reduces the spherulite size. In nonisothermal crystallization of the blend, the crystallization peak temperature moves upward slightly, but not so much in this MA–PP concentration range. Regression fitting of the nonisothermal crystallization revealed that the contribution of homogeneous nucleation, $\alpha_2(t)$, was reduced significantly with the addition of MA–PP. On the contrary, the diffusional activation energy and ψ_1 were not noticeably changed with the addition of MA–PP. Though not as certain as the E_1 and the ψ_1 calculation, the k_1 values, which is proportional to the number of effective nuclei, increased two orders when 0.2% of MA–PP was added. This shows that MA–PP is acting as a nucleating agent in the iPP phase. More details of the effect of MA–PP on the crystallization of iPP are being pursued and will be reported in the future.

4. Conclusions

The crystallization kinetics of iPP and MA–PP follow the Avrami behavior at early stages with Avrami exponents of 2.7 for iPP and 3.8 for MA–PP. This difference is ascribed to their different nucleation mechanisms, which originate from their different characteristics and differences in the number of existing heterogeneous nuclei. The half-crystallization times of MA–PP and iPP increase with crystallization temperature, but much more rapidly for iPP than for MA–PP. Nonisothermal crystallization results coincide with isothermal crystallization results. The nonisothermal crystallization data for MA–PP could be regressionally fitted with only the heterogeneous crystallization term, whereas the homogeneous nucleation term needed to be included for iPP in order to achieve good agreement with the experimental data at high cooling rates. The number of effective nuclei for MA–PP calculated from the kinetic parameters was almost ten times that for iPP. The diffusional activation energy of MA–PP was lower than that of iPP while the free energy of formation of a critical nucleus on the growing crystal surface was almost the same. From these facts, it can be concluded that MA–PP crystallizes mainly via heterogeneous nucleation at all cooling rates examined, while iPP crystallizes via both heterogeneous nucleation and homogeneous nucleation, which is noticeable when the cooling rate is high.

We speculate that the difference is due to the structural difference between MA–PP and iPP which causes a chain interaction such as hydrogen bonding between hydrolyzed maleic anhydride groups. The presence of a tiny amount of MA–PP in the iPP melt influences the crystallization of iPP. A small addition of MA–PP (0.2%) leads to a reduction of homogeneous nucleation at high cooling rates and to an increase in the number of effective nuclei. This means that MA–PP acts as a nucleating agent in the iPP phase. Further work is under way to show the details more explicitly and the results will be reported in the future.

Acknowledgements

Discussions with Dr Dong Young Kim at Polymer Materials Laboratory (KIST) and with Prof. Kwang Hee

Lee at Inha University are greatly appreciated. This work was supported by KIST (Grant No.2E15630).

References

[1] Hoshino S, Meinecke E, Power J, Stein RS, Newman S. J Polym Sci Part 1 1965;3:3041.
[2] Pratt CF, Hobbs SY. Polymer 1976;17:12.
[3] Martuscelli E, Pracella M, Volpe GD, Greco P. Makromol Chem 1984;185:1041.
[4] Janimak J, Cheng S, Zhang A, Hsieh E. Polymer 1992;33:728.
[5] Varga J. In: Karger-Kocsis J, editor. Polypropylene, vol. 1. London: Chapman and Hall, 1995. chap. 3.
[6] Galeski A. In: Karger-Kocsis J, editor. Polypropylene, vol. 1. London: Chapman and Hall, 1995. chap. 4.
[7] Avrami M. J Chem Phys 1939;7:1103.
[8] Avrami M. J Chem Phys 1941;9:117.
[9] Grenier D, Prud'homme RE. J Polym Sci: Polym Phys Ed 1980;18:1655.
[10] Avalos F, Lopez-Manchade MA, Arroyo M. Polymer 1996;37:5681.
[11] Mandelkern L, Quinn FA. J Appl Phys 1954;25:830.
[12] Simon FT, Rutherford JM. J Appl Phys 1964;35:82.
[13] Trivedi BC, Culbertson BM. Maleic anhydride. New York: Plenum Press, 1982.
[14] Seo Y, Hwang SS, Kim KU, Lee J, Hong SI. Polymer 1993;34:1667.
[15] Seo Y, Hong SM, Kim KU. Macromolecules 1997;30:2978.
[16] Seo Y, Kim B, Kwak SJ, Kim KU, Kim J. Polymer 1999;40:4441.
[17] Bodor G. Structural investigation of polymers. Chichester: Ellis Horwood, 1991.
[18] Wunderlich B. In: Turi EA, editor. Thermal characterization of polymeric materials, 2nd edn. New York: Academic Press, 1997. chap. 2.
[19] Kim YC, Kim CY, Kim SC. Polym Engng Sci 1991;31:1009.
[20] Hammami A, Mehrotra AK. Polym Engng Sci 1995;35:170.
[21] Wunderlich B. Macromolecular physics: crystal nucleation, growth, annealing, vol. 2. New York: Academic Press, 1976.
[22] Kim YC, Ahn W, Kim CY. Polym Engng Sci 1997;37:1003.
[23] Morasse B, Haudin JM. Colloid Polym Sci 1986;264:117.